

Non-linear effects in osmotic membrane transport: evaluation of the S-entropy production by volume flux of aqueous ammonia and sulfuric acid solutions under concentration polarization conditions

Izabella Slezak-Prochazka^a, Kornelia M. Batko^b, Andrzej Ślęzak^c, Wioletta M. Bajdur^d, Maria Włodarczyk-Makula^{e,*}

^aBiotechnology Centre, Silesian University of Technology, 44100 Gliwice, Akademicka 2A, Poland, email: izabella.slezak-prochazka@polsl.pl

^bDepartment of Business Informatics, University of Economics in Katowice, 2B Bogucicka, 40-287 Katowice, Poland, email: kornelia.batko@ue.katowice.pl

^cDepartment of Health Science and Physiotherapy, Jan Długosz University, 13/15 Armia Krajowa Al. 42-200 Częstochowa, Poland, email: aslezak52@gmail.com

^dFaculty of Management, Częstochowa University of Technology, 35b Armia Krajowa Al. 42-200 Częstochowa, Poland, email: wiolawb@poczta.onet.pl

^eFaculty of Infrastructure and Environment, Częstochowa University of Technology, 42-200 Częstochowa, 69 Dąbrowskiego Str, Poland, email: maria.wlodarczyk-makula@pcz.pl

Received 14 April 2022; Accepted 9 May 2022

ABSTRACT

Concentration polarization is an effect of concentration boundary layers formation by solutions transported through a membrane. The paper was aimed at determining the osmotic membrane transport of a ternary solution under concentration polarization conditions. Volume fluxes (J_{vk}^i) in a system containing a Nephrophan[®] membrane set in a horizontal plane separating water and aqueous ammonia and/or H₂SO₄ solutions were experimentally studied. The experimental results were used to evaluate the effects of concentration polarization, natural convection, and amplification of J_{vk}^i using defined coefficients. It was shown that for the homogenous solutions J_{vk}^i depends on the concentration and composition of the solutions, whereas for concentration polarization conditions, J_{vk}^i additionally depends on the configuration of the membrane system. Next, J_{vk}^i was used to assess the production of entropy for the conditions of homogeneity of solutions (Φ_{sk}^i), while J_{vk}^i was used to assess the production of entropy for concentration polarization conditions (Φ_{sk}^i). In addition, the diffusion–convective effects and the convection effect in the source of entropy were calculated. The concentration polarization coefficient ζ_i was related to a modified concentration Rayleigh number, for example, the parameter controlling the transition from the non-convective (diffusive) to the convective state. The results show that the Rayleigh number acts as a switch between two states of the concentration field: a convective with a higher entropy production and a non-convective with a lower entropy production. Therefore, membrane transport under polarization concentration conditions leads to a decrease in the entropy production. Understanding the membrane transport properties and mechanism can be used for developing and improving membrane technologies and techniques useful in medicine and in water and wastewater treatment processes.

Keywords: Osmotic membrane transport; Entropy production; Kedem–Katchalsky equations; Concentration polarization; Natural convection

* Corresponding author.

1. Introduction

Membrane transport processes occur in biological organisms and in physicochemical systems, in which a membrane constitutes a selective barrier that separates the interior of the system from the exterior. Transport processes are driven by various types of physical fields such as concentration, pressure, temperature or electric potential fields and therefore they participate in shaping the field character of nature [1,2]. Physical fields are modified by the flows generated by driving forces that may result in diffusive concentration polarization [3]. Biological membranes are used in various branches of science, technology, medicine and industry [4]. The majority of membrane materials used for osmosis-based membrane systems are either highly stable polymers, such as polybenzimidazole, polyamide, polytriazole, cellulose acetate, or biodegradable polymers such as lactic acid, bacterial cellulose, and chitosan [5–9].

Cellulose acetate was used as a film-forming material used in this study.

In thermodynamic systems, including membrane systems, internal energy (U) is converted into free energy (F) and dispersed energy (TS), where T – absolute temperature, S – entropy) according to the equation $U = F + TS$. The rate of change in the entropy of the system (dS/dt) is the sum of the rate of entropy exchange between the system and the environment (dS_e/dt) and the rate of entropy formation inside the system (dS_f/dt) [10,11]. The rate of entropy creation or production within the system is given by the expression $dS_i/dt = \int \varphi_s dV$, where φ_s – the source of entropy. In an irreversible process, φ_s is always greater than zero, and in a reversible process is equal to zero. The source of entropy φ_s determines the rate of formation of S-entropy (dS_f/dt) in the volume unit (V) of the tested system and satisfies the relation [12–14]:

$$\varphi_s = \frac{1}{T \cdot V} \frac{dS_i}{dt} = \sum_k X_k J_k > 0 \quad (1)$$

This equation shows that the set of thermodynamic forces (X_k) occurring in the system causes irreversible flows conjugated and opposite to them, measured by the fluxes J_k [8,10]. These fluxes reduce the value of the stimuli that induce them and lead the system to the state of equilibrium that exists until $\varphi_s > 0$ [12]. The product $T \cdot \varphi_s$ expresses the amount of energy dissipated per time unit and is called the dissipation function [13]. For a system containing a Δx -thick membrane that separates two homogeneous solutions of different concentrations, the source of entropy for the membrane is $\Phi_{sk} = \int_0^{\Delta x} \Phi_{sk} dx$ [11].

For concentration polarization conditions, if the solutions contain a solvent and k solutes, the global source of entropy is described by the equation [15,16].

$$\Phi_{Sk}^r = \left(\Phi_{Sk}^r \right)_{J_{sk}^r} + \sum_k \left(\Phi_{Sk}^r \right)_{J_k^r} = \frac{1}{T} J_{vk}^r \left(\Delta P \pm \sum_k \Delta \pi_k \right) + \frac{1}{T} \sum_k J_k^r \frac{\Delta \pi_k}{C_k} \quad (2)$$

where: Φ_{Sk}^r – global entropy source for the concentration polarization conditions, J_{vk}^r and J_k^r – volume and solute fluxes, respectively, for the conditions of concentration polarization of solutions, $r = A$ or B configuration of the membrane system, $\left(\Phi_{Sk}^r \right)_{J_{sk}^r}$ – S-entropy produced by J_{vk}^r , $\left(\Phi_{Sk}^r \right)_{J_k^r}$ – S-entropy produced by J_k^r , ΔP and $\Delta \pi_k = RT \Delta C_k$ – differences of hydrostatic and osmotic pressures, respectively (RT – the product of the gas constant and temperature, ΔC_k – difference of the concentration of solutions), $\bar{C}_k = (C_{hk} - C_{lk}) \left[\ln(C_{hk} C_{lk}^{-1}) \right]^{-1}$ – mean concentration of the solution in the membrane (M) or complex $l_i^r/M/l_i^r$.

In previous papers, we showed that, fluxes J_{vk}^r and J_k^r depend on the transport properties of the membrane, the configuration of the membrane system as well as the physicochemical properties and composition of solutions separated by the membrane [3,17–20]. The values of these fluxes were shown to be higher under convective conditions than under non-convective conditions [3,17]. Additionally, we described the volume J_{vk}^r and solute J_k^r fluxes as a non-linear function of the concentration gradients of the solution components for ternary solutions, that consist of water and two solutes of which one causes an increase and the other a decrease in the density as their concentration increases. As we showed previously, due to Eq. (2), the source of entropy for the concentration polarization conditions (Φ_{Sk}^r), was a non-linear function of J_{vk}^r and/or J_k^r and $\sum_k \left(\Phi_{Sk}^r \right)_{J_k^r} \gg \left(\Phi_{Sk}^r \right)_{J_{sk}^r}$ [3,15,21]. Concentration polarization can be studied using binary and ternary solutions [17]. Previously, we studied binary solutions that contained one dissolved substance such as ethanol, ammonia, potassium chloride, sodium chloride, hydrogen chloride, copper(II) sulfate or glucose as well as ternary solutions, that contained two dissolved substances, such as ethanol/glucose, ethanol/sodium chloride, ethanol/copper(II) sulfate, ammonia/potassium chloride, ammonia/hydrogen chloride [3,15–19,21].

In this paper we aim to determine the osmotic membrane transport of a ternary solutions under concentration polarization conditions. We use a single-membrane system with a membrane located in the horizontal plane separating water and a solution that consist of water, ammonia and/or sulfuric acid.

In this system, we experimentally determined fluxes J_{vk}^r and J_k^r to calculate the coefficients of amplification of the volume flux (a_k^r), convection effects (γ_k^r), the effects of concentration polarization (ζ_k^r) and the sources of entropy $\left(\Phi_{Sk}^r \right)_{J_{sk}^r}$ and $\left(\Phi_{Sk}^r \right)_{J_k^r}$. Additionally, the effect of the concentration of individual components of the solutions and the configuration of the membrane system on the value of J_v^r and J_{vk}^r was described in homogenous solutions and under conditions of concentration polarization. The obtained results show that osmotic fluxes are amplified for ternary compared to binary solutions in a studied membrane system and that the entropy production non-linearly depend on a concentration difference.

We also showed that the Rayleigh number, for example, the parameter controlling the transition from the non-convective (diffusive) to the convective state, acts as a switch between a convective and a non-convective state. Therefore, membrane transport leads to a decrease in the entropy

production under polarization concentration conditions. Membrane transport properties, showed in this paper, can be applied to improve membrane technologies in medicine as well as in water and wastewater treatment processes.

2. Model of the membrane system

The membrane system used as a model for volume transport is illustrated schematically in Fig. 1 [3,20]. In this system, a neutral, symmetrical, isotropic and selective membrane (*M*) situated in the horizontal plane separates two solutions with the initial concentrations C_{hk} and C_{lk} ($C_{hk} > C_{lk}$, $k = 1, 2$). In configuration A, a solution with a concentration C_{lk} is localized in the compartment above the membrane and a solution with a concentration C_{hk} is localized in the compartment below the membrane. In configuration B, locations of solutions with concentration C_{lk} and C_{hk} are reversed. If it is assumed that the driving force for osmotic flows is the difference in concentrations between the solutions filling the upper and lower compartments, then for the configuration A, $\Delta C_k > 0$, and for the configuration B, $\Delta C_k < 0$.

According to the laws of diffusion, water and dissolved substances penetrating through the membrane form concentration boundary layers (CBLs) indicated by l_h^r and l_l^r ($r = A, B$) on both sides of the membrane. The phenomenon of creating CBLs is called concentration polarization. The thickness of a concentration boundary layer l_h^r is indicated by δ_h^r and the thickness of a l_l^r is indicated by δ_l^r . In non-convection conditions, these thicknesses increase with time according to the dependencies $\delta_h^r = k_h t^{0.5}$ and $\delta_l^r = k_l t^{0.5}$, where k_h and k_l are experimentally determined constants [23–25]. For aqueous ethanol solutions and $t = 2,500$ s, the thickness of these layers is about 5 mm [23]. The creation of these layers leads to a decrease in the concentration difference from the value of $C_{hk} - C_{lk}$ to the value of $C_{hk}^r - C_{lk}^r$, where $C_{hk}^r > C_{lk}^r$, $C_{hk} > C_{hk}^r$ and $C_{lk}^r > C_{lk}$.

When the solution of lower density is placed in the compartment under the membrane, and the solution of higher density in the compartment above, the $l_h^r M / l_l^r$ complex loses hydrodynamic stability and, consequently, free convection may occur in the adjacent areas [25,26]. When the

thicknesses of the concentration layers δ_h^r and δ_l^r reach the critical thickness ($(\delta_h^r)_{crit}$ and $(\delta_l^r)_{crit}$) and the concentration Rayleigh numbers ((R_{Cl}^r, R_{Cl})), that control the process of natural convection, reach critical values, hydrodynamic instabilities occur [27]. As previously shown [26], $(\delta_l^r)_{crit}$ reaches the value of 0.5–1 mm. Over time, the destructive effect of natural convection limits the growth of δ_h^r and δ_l^r and accelerates the diffusion of the substance beyond the layers, which extends the effect of convection to the entire volume of the solution. Under certain conditions, even liquid structuring may occur, which is manifested by the appearance of plum structures [28,29]. The process of creating CBLs can be visualized by optical methods [23,24].

The process of creation of CBLs is accompanied by a decrease in values of the volume flux [18,19]. Their measure is the volume fluxes (J_{vk}^r, J_{vk}^l), which can be described by the Kedem–Katchalsky equation for homogeneous and concentration polarization conditions [18]

$$J_{vk} = L_p \Delta P \pm L_p RT \sum_k \varepsilon_k \sigma_k \Delta C_k \tag{3}$$

$$J_{vk}^r = \zeta_p^r L_p \Delta P \pm \zeta_p^r L_p RT \sum_k \zeta_v^r \varepsilon_k \sigma_k \Delta C_k \tag{4}$$

where L_p and σ_k – hydraulic permeability and reflection coefficients, ε_k ($1 \leq \varepsilon_k \leq 2$) – the Van’t Hoff coefficient (for non-dissociating substances $\varepsilon_k = 1$, and for fully dissociated substances $\varepsilon_k = 2$), ζ_p^r and ζ_v^r are the hydraulic and osmotic concentration polarization coefficients, respectively, ΔP – hydrostatic and osmotic pressure differences, respectively, RT – the product of the gas constant and the absolute temperature, ΔC_k – concentration difference ($r = A, B; k = 1, 2, \dots, n$). The first components of Eqs. (3) and (4) relate to hydraulic volume fluxes, and the second – to osmotic volume fluxes.

To show the relationship between the J_{vk}^r and J_{vk}^l fluxes for configurations A and B of the membrane system ($r = A, B$), the following expressions were defined by Eqs. (3) and (4).

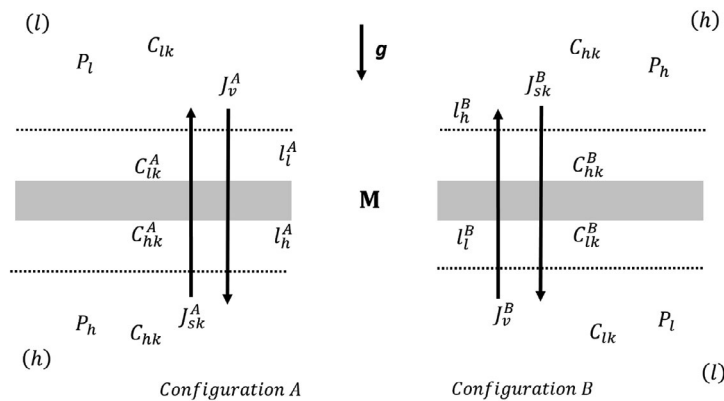


Fig. 1. Model of single-membrane system: *M* – membrane, *g* – gravitational acceleration, l_h^A and l_l^A – the concentration boundary layers in configuration A, l_h^B and l_l^B – the concentration boundary layers in configuration B, P_h and P_l – mechanical pressures, C_{hk} and C_{lk} – global solution concentrations ($C_{hk} > C_{lk}$), $C_{lk}^A, C_{hk}^A, C_{lk}^B$ and C_{hk}^B – local (at boundaries between membrane and CBLs) solution concentrations, J_{vk}^A – solute and volume fluxes in configuration A, J_{vk}^B – solute and volume fluxes in configuration B, ($k = 1$ or 2) [20].

$$\gamma_{vk} = \frac{J_{vk}^A - J_{vk}^B}{J_{vk}} \quad (5)$$

The values of the γ_{vk} coefficients show the influence of concentration polarization and gravitational convection on membrane transport. These coefficients can be a measure of the distance of convective processes from the critical (non-convection) state and meet the criterion: $1 \leq \gamma_{vk} \leq 1$. In the critical state $\gamma_{vk} = 0$. It means that $J_{vk}^A = J_{vk}^B$ ($k = 1$ or 2). The condition $\gamma_{vk} = +1$ is fulfilled if $J_{vk}^A = 0$ and $J_{vk}^B = J_{vk}$, whereas $\gamma_{vk} = -1$ is true if $J_{vk}^B = 0$ and $J_{vk}^A = J_{vk}$.

If the solutions contain a solvent and k of dissolved substances, then the source of entropy generated by volume flows, corresponding to the conditions of homogeneity of solutions, is described by the equation [12,15,16].

$$(\Phi_{Sk})_{J_{vk}} = \frac{1}{T} J_{vk} \left(\Delta P \pm \sum_{k=1}^2 \varepsilon_k \Delta \pi_k \right) \quad (6)$$

where $(\Phi_{Sk})_{J_{vk}}$ is the S-entropy produced by J_{vk}^A, J_{vk}^B – volume flux for the homogeneity conditions of the solutions, ΔP and $\Delta \pi_k$ – differences in hydrostatic and osmotic pressures, ε_k ($1 \leq \varepsilon_k \leq 2$) – the Van't Hoff coefficient ($k = 1$ or 2).

Under real conditions, the homogeneity of the solutions is disturbed by the concentration polarization, that results in CBLs that are spontaneously formed on both sides of the membrane. For the conditions of concentration polarization, Eq. (6) takes the form [15,16]:

$$(\Phi_{Sk}^r)_{J_{vk}^r} = \frac{1}{T} J_{vk}^r \left(\Delta P \pm \sum_{k=1}^2 \varepsilon_k \Delta \pi_k \right) \quad (7)$$

where $(\Phi_{Sk}^r)_{J_{vk}^r}$ is the S-entropy produced by J_{vk}^A, J_{vk}^B – volume flux for the concentration polarization conditions of

solutions, $r = A$ or B means the configuration of the membrane system and ($k = 1$ or 2).

3. Methodology for measuring the volume flux

The study of the volume fluxes (J_{vk}^A, J_{vk}^B) were carried out using the measuring set presented in Fig. 2 and described in the previous papers [27,30].

Briefly, the set consisted of two cylindrical measuring vessels (h, l) with a volume of 200 cm³ each. The vessel h contained the tested binary or ternary solution, while the vessel l contained pure water. Aqueous solutions of ammonia (NH₃·H₂O) or aqueous solutions of H₂SO₄ were used as binary solutions. The ternary solutions were solutions of ammonia in an aqueous solution of H₂SO₄ or solutions of H₂SO₄ in an aqueous solution of ammonia. The density of aqueous ammonia solutions is lower than the density of water, and the density of the aqueous solution of H₂SO₄ is greater than the density of water. However, the density of ammonia solutions in the aqueous solution of H₂SO₄ and the density of the solutions of H₂SO₄ in the aqueous ammonia solution may be lower, equal to, or greater than the density of water. For the conditions of concentration polarization, the value of the volume flux of aqueous solutions of ammonia and sulfuric acid depends on the density of the solutions separated by the membrane, because restoration of the density gradient in respect to g determines the stability or instability of CBLs. The vessels h and l were separated by a synthetic polymeric biomembrane (Nephrophan®, VEB Filmfabrik, Wolfen, Germany) with an area surface of $A = 3.36$ cm². Nephrophan is a microporous, highly hydrophilic membrane made of regenerated cellulose and used in hemodialyzers [31]. Transport properties of Nephrophan® were determined according to the Kedem and Katchalsky formalism by the following coefficients: hydraulic permeability (L_p), reflection (σ) and permeability diffusion (ω) [12]. The values of these coefficients for aqueous solutions of ammonia (index 1) and H₂SO₄ (index 2), determined in a series of independent

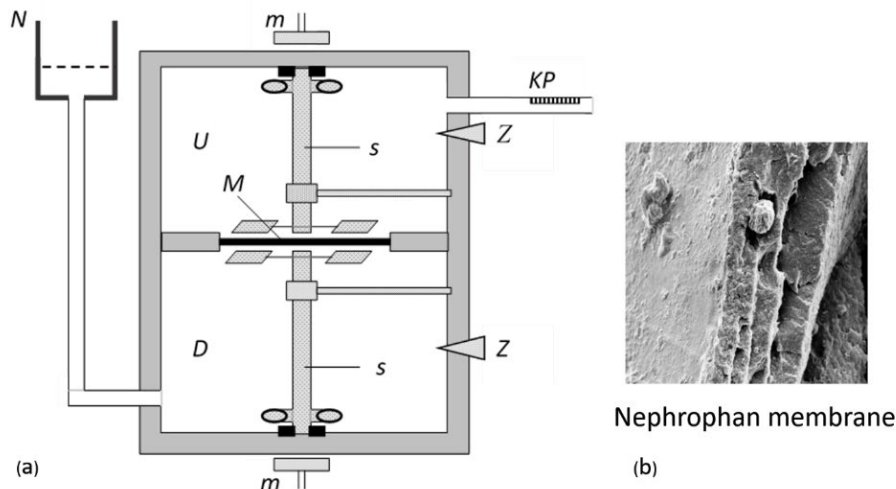


Fig. 2. Measuring system (h, l – measuring vessels, N – external solution tank, s – mechanical stirrers, M – membrane, K – calibrated pipette, m – magnets, z – plugs) [22]. (b) Images of cross-section nephrophan membrane obtained from scanning electron microscope (magnification 10,000 times) [22].

experiments, were: $L_p = 5 \times 10^{-12} \text{ m}^3 \text{ N}^{-1} \text{ s}^{-1}$, $\sigma_1 = 0.01$, $\sigma_2 = 0.05$, $\omega_1 = 2.7 \times 10^{-9} \text{ mol N}^{-1} \text{ s}^{-1}$ and $\omega_2 = 6.1 \times 10^{-9} \text{ mol N}^{-1} \text{ s}^{-1}$. The membrane was situated in the horizontal plane, that is, perpendicular to the gravitational acceleration (\mathbf{g}) and parallel or antiparallel to the density gradient ($\Delta\rho$) [17]. For small concentration (C_k) the dependence of density on concentration is linear, so $\Delta\rho = \sum_k \frac{\partial\rho}{\partial C_k} C_k$, where $\frac{\partial\rho}{\partial C_k} > 0$ or $\frac{\partial\rho}{\partial C_k} < 0$. Only this position of the membrane makes it possible to evaluate the effects of concentration polarization and the effects of free convection in volume fluxes.

The vessel with a the test solution was connected to a graduated pipette (KP), placed in a plane parallel to the plane of the membrane. The graduated pipette was used to measure the increase in volume of the solution (ΔV) in the vessel h . A vessel with water connected to a water reservoir (N) with adjustable height relative to the pipette was used to compensate for the hydrostatic pressure ($\Delta P = 0$) present in the measurement set.

The studies of J_{vk} and J_{vk}^r were carried out according to the procedure described in the previous paper [17]. Each experiment was performed for configurations A and B of the membrane system in two stages. In the first stage, the study of volume flux (J_{vk}) was carried out under the conditions of intensive stirring of the solutions separated by the membrane with the use of mechanical stirrers. In the second-stage, volume fluxes (J_{vk}^r) were examined after switching off the mechanical stirring. At each stage, the tests were carried out until steady states of the volume fluxes were obtained. Switching off the mechanical stirring of the solutions causes a transition from the conditions of homogeneity to the conditions of concentration polarization of solutions characterized by CBLs created on both sides of the membrane. These layers are destroyed under conditions that favor the occurrence of natural convection processes, controlled by the Rayleigh concentration number [25–27]. Therefore, membrane transport is usually osmotic-diffusion-convective in unstable conditions.

All studies of J_{vk} and J_{vk}^r fluxes were carried out in isothermal conditions at $T = 295 \text{ K}$. The volume flux was calculated based on measurements of the volume change (ΔV) in the pipette over time Δt through the membrane area surface (A), using the formula $J_{vk} = (\Delta V)A^{-1}(\Delta t)^{-1}$, for conditions $\Delta P = 0$. J_{vk} and J_{vk}^r always occurred from the solution with a lower concentration to the solution with a higher concentration. To distinguish volume fluxes in or against the acceleration due to gravity (\mathbf{g}), the following convention was adopted: if J_{vk}^r and \mathbf{g} are parallel, a negative sign of J_{vk}^r and a negative sign of $\Delta\pi$ were assumed, whereas if J_{vk}^r and \mathbf{g} are opposite, a positive sign of J_{vk}^r and a positive sign of $\Delta\pi$ were assumed.

To study volume fluxes in both configurations of the membrane system, the time dependences of the J_{vk} and J_{vk}^r were determined for different concentrations and compositions of solutions. Each measurement series was performed in triplicate. The relative error in determining J_{vk}^r and J_{vk} was not greater than 5%. Based on the characteristics $J_{v1}^r = f(t)$, $J_{v1} = f(t)$, $J_{v2}^r = f(t)$ and $J_{v2} = f(t)$, for the steady state, the characteristics $J_{v1}^r = f(\Delta C_1, \Delta C_2 = \text{const.})$, $J_{v1} = f(\Delta C_1, \Delta C_2 = \text{const.})$, $J_{v2}^r = f(\Delta C_2, \Delta C_1 = \text{const.})$ and $J_{v2} = f(\Delta C_2, \Delta C_1 = \text{const.})$.

4. Results and discussion

4.1. Concentration dependencies of the volume flux for conditions of homogeneity of solutions

The dependencies $J_{v1} = f(\Delta C_1, \Delta C_2 = \text{const.})$ and $J_{v2} = f(\Delta C_2, \Delta C_1 = \text{const.})$ were plotted for homogeneity conditions of solutions (Figs. 3a and b). Homogeneity conditions were obtained by mechanical stirring of the solutions at a speed of 500 rpm. For binary solutions (graphs 1) the dependencies $J_{v1} = f(\Delta C_1, \Delta C_2 = 0)$ and $J_{v2} = f(\Delta C_2, \Delta C_1 = 0)$ were linear. For ternary solutions the dependencies $J_{v1} = f(\Delta C_1, \Delta C_2 = 100 \text{ mol m}^{-3})$, $J_{v1} = f(\Delta C_1, \Delta C_2 = 200 \text{ mol m}^{-3})$ and $J_{v1} = f(\Delta C_1, \Delta C_2 = 300 \text{ mol m}^{-3})$, as well as the dependencies $J_{v2} = f(\Delta C_2, \Delta C_1 = 250 \text{ mol m}^{-3})$, $J_{v2} = f(\Delta C_2, \Delta C_1 = 500 \text{ mol m}^{-3})$ and $J_{v2} = f(\Delta C_2, \Delta C_1 = 750 \text{ mol m}^{-3})$ should also be linear, shifted from the graphs 1 by the value J_{v1} or J_{v2} obtained for the appropriate and fixed values of ΔC_2 or ΔC_1 . This means that the J_{v1} or J_{v2} fluxes should be the sum of the fluxes caused by ΔC_1 and ΔC_2 . However, this is not true, because this flux is the sum of the fluxes caused by ΔC_2 and twice the flux caused by ΔC_1 . This means that aqueous ammonia solutions ($\text{NH}_3 \cdot \text{H}_2\text{O}$) behave like non-electrolytes: 100 mol m⁻³ aqueous ammonia solution at 18°C consists of 46.2% NH_3 , 52.4% NH_4OH ($\text{NH}_3 \cdot \text{H}_2\text{O}$) and 1.4% $[\text{NH}_4]^+$ [32]. Moreover, as the concentration of the solutions increases, the degree of dissociation decreases. Therefore, the difference in the osmotic pressure of $\text{NH}_3 \cdot \text{H}_2\text{O}$ in the binary solution is $\Delta\pi_1 = RT\Delta C_1$. In ternary solutions, in the presence of a strong electrolyte, such as an aqueous solution of H_2SO_4 , the following process likely takes place: $2(\text{NH}_3 \cdot \text{H}_2\text{O}) + \text{H}_2\text{SO}_4 \leftrightarrow 2\text{NH}_4\text{OH} + \text{H}_2\text{SO}_4 \leftrightarrow (\text{NH}_4)_2\text{SO}_4 + 2\text{H}_2\text{O} \leftrightarrow 2[\text{NH}_4]^+ + [\text{SO}_4]^{2-} + 2\text{H}^+ + 2\text{O} \text{H}^-$. This means that the presence of H_2SO_4 causes complete dissociation of NH_4OH and an increase in the osmotic pressure difference to the value of $\Delta\pi_1 = RT\Delta C_1$. In contrast, H_2SO_4 , a strong electrolyte, occurs in a dissociated form both in binary and ternary solutions. Therefore, the difference of the osmotic pressure of H_2SO_4 is $\Delta\pi_2 = 2RT\Delta C_2$.

4.2. Concentration dependence of the volume flux for concentration polarization conditions

The dependency $J_{v1}^A = f(\Delta C_1, \Delta C_2 = \text{const.})$ was plotted for A ($r = A$) configuration and $J_{v1}^B = f(\Delta C_1, \Delta C_2 = \text{const.})$ for B ($r = B$) configuration of the membrane system (Fig. 3c). Accordingly, the dependency $J_{v2}^A = f(\Delta C_2, \Delta C_1 = \text{const.})$ was plotted for A ($r = A$) configuration and $J_{v2}^B = f(\Delta C_2, \Delta C_1 = \text{const.})$ for B ($r = B$) configuration of the membrane system (Fig. 3d). Curves 1A and 1B in Fig. 3c show that an increase in the value of ΔC_1 in binary solutions ($\Delta C_2 = 0$) causes a linear increase of the J_{v1}^A and J_{v1}^B ($J_{v1}^A > J_{v1}^B$). On the contrary, the characteristics 3A and 3B, 4A and 4B as well as 5A and 5B obtained for ternary solutions were shown to be non-linear. For configuration A, an increase in the value of ΔC_1 in ternary solutions ($\Delta C_2 > 0$) causes a non-linear increase in the value of the J_{v1}^A flux, and in the configuration B, a step decrease followed by an increase in the value of the J_{v1}^B flux. Moreover, an increase in the value of ΔC_2 shifts the 3A curve in respect to the 2A curve and shifts the 4A curve in respect to the 3A curve by $\Delta(\Delta C_1) \cong 394 \text{ mol m}^{-3}$. Additionally, an increase in the

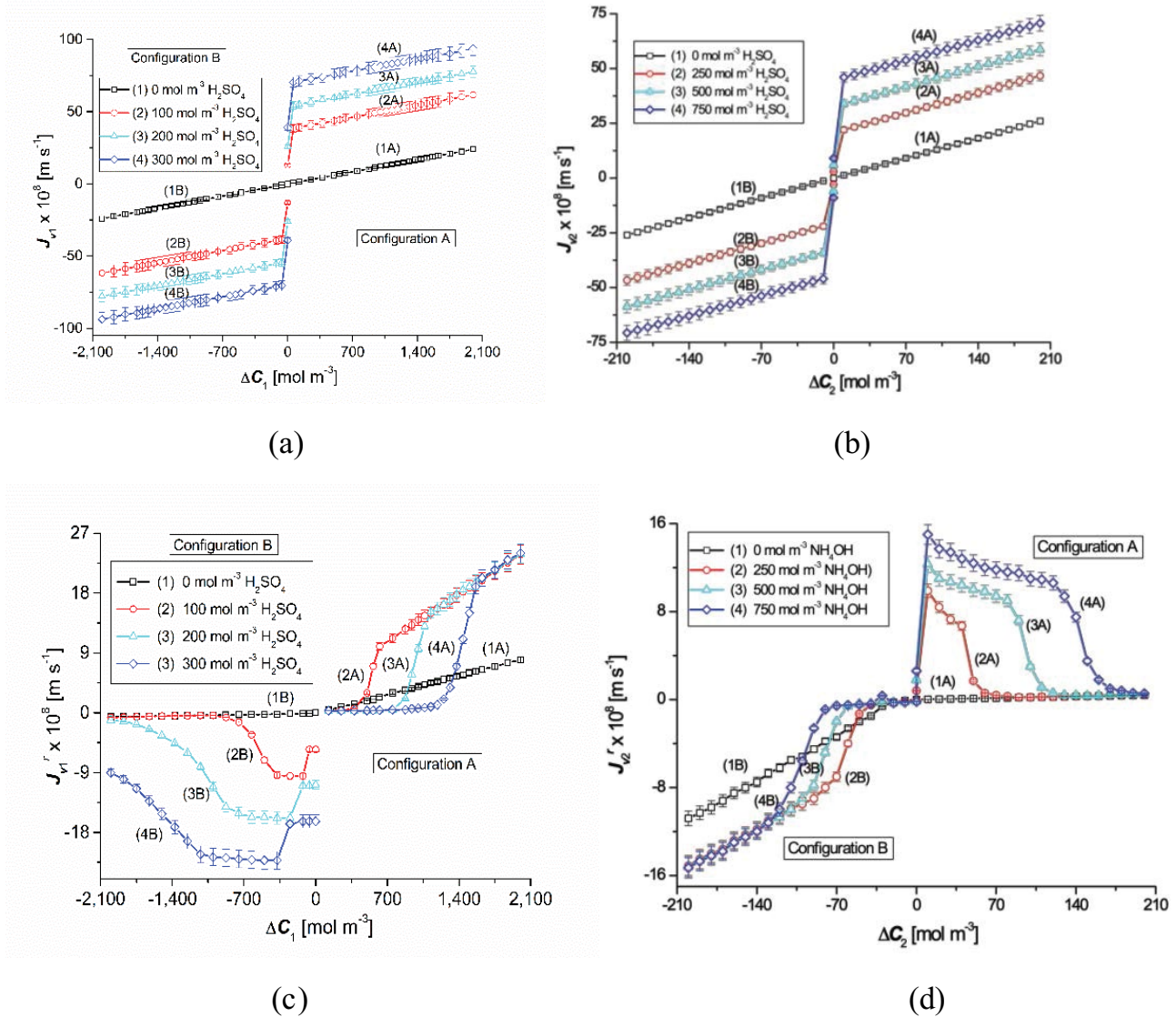


Fig. 3. Concentration dependencies of the volume flux for the conditions of homogeneity and polarization of solutions separated by the membrane. Experimental dependence $J_{v1} = f(\Delta C_1, \Delta C_2 = \text{const.})$ for the conditions of homogeneity of (a) NH_4OH solution in aqueous H_2SO_4 solution and (b) H_2SO_4 solution in aqueous NH_4OH solution. Experimental dependence $J_{v1}^r = f(\Delta C_1, \Delta C_2 = \text{const.})$, ($r = A, B$) for the concentration polarization conditions of (c) NH_4OH solution in aqueous H_2SO_4 solution and (d) H_2SO_4 solution in aqueous NH_4OH solution.

value of ΔC_2 shifts the 3B curve in respect to 2B curve by $-\Delta(\Delta C_1) \cong 678 \text{ mol m}^{-3}$ and shifts the 4B curve in respect to the 3B curve by $-\Delta(\Delta C_1) \cong 743 \text{ mol m}^{-3}$.

Curves 1A and 1B in Fig. 2d show that the increase in the value of ΔC_2 in binary solutions ($\Delta C_1 = 0$) causes a linear increase of J_{v2}^A and J_{v2}^B ($J_{v2}^A < J_{v2}^B$). On the contrary, the characteristics 3A and 3B, 4A and 4B as well as 5A and 5B obtained for ternary solutions are non-linear. For configuration A an increase in the value of ΔC_2 in ternary solutions ($\Delta C_1 > 0$) causes a step increase and then a non-linear decrease in the value of the J_{v2}^A flux, while in the configuration B – a decrease in the value of the J_{v2}^B flux. Moreover, an increase in the value of ΔC_1 shifts the 4A curve in relation to the 3A curve and also shifts the 5A curves in relation to the 4A curves by $\Delta(\Delta C_1) \cong 52 \text{ mol m}^{-3}$. Additionally, an increase

in the value of ΔC_1 shifts the 4B curve in relation to the 3B curve and also shifts the 5B curve in relation to the 4B curve by $-\Delta(\Delta C_1) \cong 15 \text{ mol m}^{-3}$, with a simultaneous increase in the value of J_{v2}^B . Moreover, the curves 2A, 3A, 4A and 5A as well as the curves 2B, 3B, 4B and 5B shown in Figs. 3A and 3B are centrally asymmetric with respect to the point with the coordinates (0, 0), which is caused by partial destruction of CBLs by natural convection [17,33].

The hydrodynamics of CBLs in particular configurations of the membrane system under membrane transport conditions should be considered when analyzing the characteristics $J_{v1}^r = f(\Delta C_1, \Delta C_2 = \text{const.})$ and $J_{v2}^r = f(\Delta C_2, \Delta C_1 = \text{const.})$ shown in Figs. 3C and 3D. Hydrodynamic instabilities appear for sufficiently high concentrations of ammonia or H_2SO_4 when the aqueous ammonia solution (index 1) is

in the compartment below the membrane (configuration A) and the aqueous solution of H_2SO_4 (index 2) is in the compartment above the membrane (configuration B). Such instabilities are not observed even for high values of ΔC_1 (in the case of aqueous ammonia solutions) or ΔC_2 (in the case of aqueous H_2SO_4 solutions) when the aqueous ammonia solution is in the compartment above the membrane (configuration B) and the aqueous solution of H_2SO_4 is in the compartment under the membrane (configuration A). The characteristics $J_{v1}^r = f(\Delta C_1, \Delta C_2 = 0)$ and $J_{v2}^r = f(\Delta C_2, \Delta C_1 = 0)$ obtained for binary solutions in configurations A and B clearly differ due to the different conditions of reaching the steady states J_{v1}^r and J_{v2}^r . The slope of the characteristic $J_{v1}^r = f(\Delta C_1, \Delta C_2 = 0)$ for configuration A is greater than in configuration B as expected due to the occurring hydrodynamic instabilities. For the same reason, the slope of the characteristic $J_{v2}^r = f(\Delta C_2, \Delta C_1 = 0)$, for configuration B is greater than for configuration A. This is due to the fact that hydrodynamic instabilities observed in configuration A for aqueous ammonia solutions, and in configuration B for water solutions of H_2SO_4 , cause destruction of CBLs and improve membrane transport.

Adding H_2SO_4 to an aqueous solution of ammonia or ammonia to an aqueous solution of H_2SO_4 , influences, by changing the density of the solutions, the conditions of occurrence of hydrodynamic instabilities. H_2SO_4 causes an increase, while ammonia a decrease in the density of solutions with an increase in their concentration. Therefore, hydrodynamic instabilities are observed at higher concentrations of ammonia or H_2SO_4 in the configuration A of a membrane system containing ammonia solutions in H_2SO_4 aqueous solution and in the configuration B of a membrane system containing H_2SO_4 solutions in aqueous ammonia solution. This is manifested by lower values of J_{v1}^A for small ΔC_1 or smaller values $|J_{v2}^B|$ for small $|\Delta C_2|$ compared to the binary solution. The appearance of hydrodynamic instabilities in both compartments can be associated with the ΔC_1 range, in which a rapid increase of J_{v1}^A is observed in the steady state, and with the $|\Delta C_2|$ range, in which a rapid increase in the value of $|J_{v2}^B|$ is observed in the steady state.

For higher values of ΔC_2 , the observed increase in the value of J_{v1}^A occurs at higher values of ΔC_1 . Further increase of ΔC_1 leads to a transition of the characteristic $J_{v1}^A = f(\Delta C_1, \Delta C_2 = \text{const.})$ to the linear range to which all the characteristics tend for different ΔC_2 . However, the higher ΔC_2 , the later the characteristic approaches a common linear range at higher ΔC_1 . In contrast, an observed increase in value $|J_{v2}^B|$ occurs for higher values $|\Delta C_1|$ and lower values of $|\Delta C_2|$. Further increasing $|\Delta C_2|$ leads to the transition of the characteristic $J_{v2}^B = f(\Delta C_2, \Delta C_1 = \text{const.})$ into the linear range to which all the characteristics pursue for different $|\Delta C_1|$. The greater $|\Delta C_1|$, the later the characteristic approaches the common linear range with smaller $|\Delta C_2|$. Values of J_{v1}^A are greater for ternary solutions compared to J_{v1}^A for binary solutions for the same ΔC_1 and values of $|J_{v2}^B|$ are greater for ternary solutions compared to $|J_{v2}^B|$ for binary solutions for the same $|\Delta C_2|$. This is associated with larger amounts of molecules in the solution, and thus with a larger osmotic stimulus ΔC_1 and larger $|\Delta C_2|$. The non-linear transition in the characteristics $J_{v1}^r = f(\Delta C_1, \Delta C_2 = \text{const.})$ and $J_{v2}^B = f(\Delta C_2, \Delta C_1 = \text{const.})$ can be related to a gradually

increasing influence of hydrodynamic instabilities on the transport in a membrane system. The linear range for higher ΔC_1 and higher $|\Delta C_2|$ can be related to the intense (steady, saturated) nature of hydrodynamic instabilities in the membrane system, responsible for the increase of the osmotic membrane transport.

The situation is different for B configuration of the membrane system containing ammonia solutions in an aqueous H_2SO_4 solution and in the A configuration of the membrane system containing H_2SO_4 solutions in the aqueous ammonia solution. Adding H_2SO_4 to aqueous ammonia solutions in the B configuration, and adding ammonia to aqueous H_2SO_4 solutions in the A configuration, causes hydrodynamic instabilities in the system, resulting in a significant separation of the characteristics $J_{v1}^B = f(\Delta C_1, \Delta C_2 = \text{const.})$ and $J_{v2}^A = f(\Delta C_2, \Delta C_1 = \text{const.})$ for ternary solutions from the characteristics for binary solutions, already for small values of ΔC_1 and $|\Delta C_2|$, respectively. Increasing the value of ΔC_1 , with a fixed ΔC_2 or $|\Delta C_2|$ at fixed $|\Delta C_1|$ causes a significant deviation in the characteristics for the ternary solution compared to the characteristics for the binary solution. Further increase of ΔC_1 or $|\Delta C_2|$ causes, upon the range of stable influence of hydrodynamic instabilities, almost the same value of J_{v1}^B and J_{v2}^A for the ternary solution and gradual approaching of the characteristics for ternary and binary solutions. This may be related to the gradual reduction of the influence of hydrodynamic instabilities on membrane transport until they are completely eliminated with sufficiently large ΔC_1 or $|\Delta C_2|$ which leads to the overlapping of the characteristics for the binary and ternary solutions. Increase in ΔC_2 or $|\Delta C_1|$ causes the extension of the ternary solution characteristic towards higher ΔC_1 or $|\Delta C_2|$ while increasing the observed maximum volume fluxes, which can be explained by the greater intensity of hydrodynamic instabilities in the compartments of the membrane system.

4.3. Concentration polarization effect

The effect of concentration polarization of the solutions separated by the membrane positioned in the horizontal plane in relation to the volume osmotic fluxes result from the comparison of the characteristics $J_{v1}^r = f(\Delta C_1, \Delta C_2 = \text{const.})$ and $J_{v1}^r = f(\Delta C_1, \Delta C_2 = \text{const.})$, and $J_{v2}^r = f(\Delta C_2, \Delta C_1 = \text{const.})$ and $J_{v2}^r = f(\Delta C_2, \Delta C_1 = \text{const.})$. The measure of this effect is the concentration polarization coefficient denoted by ζ_{vk}^r , ($k = 1, 2$ and $r = A, B$), the definition of which is presented in the expression

$$\zeta_{vk}^r = \frac{J_{vk}^r}{J_{vk}} \quad (8)$$

where J_{vk}^r, J_{vk} – volume fluxes, respectively, for the conditions of concentration polarization and homogeneity of solutions, caused by the same change in concentration ΔC_k . The superscript $r = A, B$ denotes the configuration of the membrane system, while the subscript $k = 1, 2$ refers to the solution component.

The calculated results of the ζ_{v1}^r coefficient shown in Fig. 4a using curves 1A–4A and curves 1B–4B were obtained based on Eq. (8), taking into account the

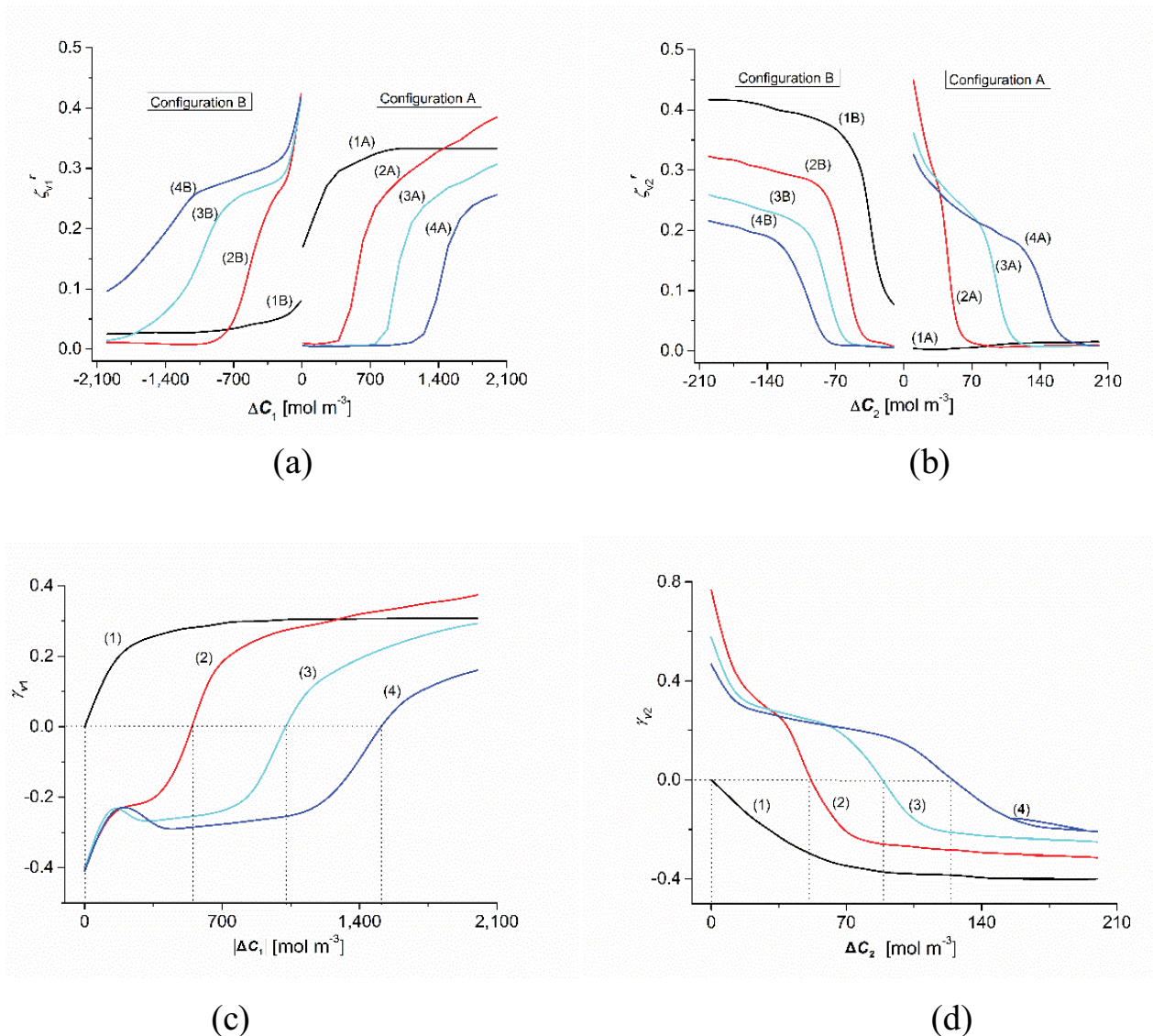


Fig. 4. Effects of concentration polarization and convection. (a) The dependence $\zeta_{v1}^A = f(\Delta C_1, \Delta C_2 = \text{const.})$, (curves 1A–4A) and $\zeta_{v1}^B = f(\Delta C_1, \Delta C_2 = \text{const.})$, (curves 1B–4B) for NH_4OH solutions in H_2SO_4 aqueous solutions and configurations A and B of the membrane system. Curves 1A and 1B obtained for $\Delta C_2 = 0$, curves 2A and 2B for $\Delta C_2 = 100 \text{ mol m}^{-3}$, curves 3A and 3B for $\Delta C_2 = 200 \text{ mol m}^{-3}$ and curves 4A and 4B for $\Delta C_2 = 300 \text{ mol m}^{-3}$. (b) The dependence $\zeta_{v2}^A = f(\Delta C_1, \Delta C_2 = \text{const.})$, (curves 1A–4A) and $\zeta_{v2}^B = f(\Delta C_1, \Delta C_2 = \text{const.})$, (curves 1B–4B), for H_2SO_4 solutions in NH_4OH aqueous solutions and configurations A and B of the membrane system. Curves 1A and 1B were obtained for $\Delta C_1 = 0$, curves 2A and 2B for $\Delta C_1 = 250 \text{ mol m}^{-3}$, curves 3A and 3B – for $\Delta C_1 = 500 \text{ mol m}^{-3}$ and curves 4A and 4B – for $\Delta C_1 = 750 \text{ mol m}^{-3}$. (c) The dependence $\gamma_{v1} = f(\Delta C_1, \Delta C_2 = \text{const.})$ for NH_4OH solutions in an aqueous H_2SO_4 solution and configurations A and B of the membrane system. Curve 1 obtained for $\Delta C_2 = 0$, curve 2 – for $\Delta C_2 = 100 \text{ mol m}^{-3}$, curve 3 – for $\Delta C_2 = 200 \text{ mol m}^{-3}$ and curve 4 – for $\Delta C_2 = 300 \text{ mol m}^{-3}$. (d) The dependence $\gamma_{v2} = f(\Delta C_2, \Delta C_1 = \text{const.})$ for H_2SO_4 solutions in NH_4OH aqueous solution and A and B configurations of the membrane system. Curve 1 was obtained for $\Delta C_1 = 0$, curve 2 – for $\Delta C_1 = 250 \text{ mol m}^{-3}$, curve 3 – for $\Delta C_1 = 500 \text{ mol m}^{-3}$, and curve 4 – for $\Delta C_1 = 750 \text{ mol m}^{-3}$.

characteristics shown in Figs. 3A and 3C. For curves 2A and 2B, the values of the coefficients ζ_{v1}^A for $\Delta C_1 = 562.3 \text{ mol m}^{-3}$ and ζ_{v1}^B for $\Delta C_1 = -562.3 \text{ mol m}^{-3}$ are the same and equal to $\zeta_{v1}^A = \zeta_{v1}^B = 0.12$. Similarly, for the curves 3A and 3B the values of the coefficients ζ_{v1}^A for $\Delta C_1 = 791.8 \text{ mol m}^{-3}$ and ζ_{v1}^B for $\Delta C_1 = -791.8 \text{ mol m}^{-3}$ are the same and equal to $\zeta_{v1}^A = \zeta_{v1}^B = 0.15$. Finally, for curves 4A and 4B the values of the coefficients ζ_{v1}^A for $\Delta C_1 = 1,514.7 \text{ mol m}^{-3}$ and ζ_{v1}^B for $\Delta C_1 = -1,514.7 \text{ mol m}^{-3}$ are the same and equal to $\zeta_{v1}^A = \zeta_{v1}^B = 0.17$.

The concentration dependencies of the ζ_{v2}^r coefficient illustrated in Fig. 4b using the curves 1A–4A and curves 1B–4B, were obtained by including the characteristics shown in Figs. 3B and 3D in Eq. (8). For curves 2A and 2B, the values of the coefficients ζ_{v2}^A for $\Delta C_2 = 51.9 \text{ mol m}^{-3}$ and ζ_{v2}^B for $\Delta C_2 = -51.9 \text{ mol m}^{-3}$ are the same and equal to $\zeta_{v2}^A = \zeta_{v2}^B = 0.06$. Similarly, for curves 3A and 3B, the values of the coefficients $\zeta_{v2}^A \cdot \Delta C_2 = 89.1 \text{ mol m}^{-3}$ and ζ_{v2}^B for $\Delta C_2 = -89.1 \text{ mol m}^{-3}$ are the same and equal to $\zeta_{v2}^A = \zeta_{v2}^B = 0.16$.

Finally, for curves 4A and 4B the values of the coefficients ζ_{v2}^A for $\Delta C_2 = 123.6 \text{ mol m}^{-3}$ and ζ_{v2}^B for $\Delta C_1 = -123.6 \text{ mol m}^{-3}$ are the same and equal to $\zeta_{v2}^A = \zeta_{v2}^B = 0.16$.

As shown in Figs. 4a and 4b, when $\zeta_{vk}^A = \zeta_{vk}^B = (\zeta_{vk})_{\text{lim}}$ ($k = 1, 2$), volume osmotic transport is independent of the configuration of the membrane system ($J_{vk}^A = J_{vk}^B$). This means that for $\zeta_{vk}^A < (\zeta_{vk})_{\text{lim}}$ the CBLs system is in non-convection conditions and therefore is hydrodynamically stable, whereas for $\zeta_{vk}^A > (\zeta_{vk})_{\text{lim}}$ the CBLs system is in convective conditions and therefore is hydrodynamically unstable.

A common feature of the relationship between the concentrations of J_{vk}^r in aqueous solutions of H_2SO_4 and/or ammonia is the change in the nature of transport from diffusion-osmotic to osmotic-diffusion-convective or vice versa. Therefore, under the conditions of the Earth's gravitational field and concentration field, gravitational convection appears or disappears depending on the density of the solutions separated by the membrane, the measure of the effect of gravitational convection is the positive or negative coefficient γ_{vk} . A positive value of this coefficient indicates that the convective movements that destroy the CBL are vertically downward, and negative that they are vertically upward. The transition from non-convective to convective or vice versa has the characteristics of a pseudo-phase transition.

4.4. Convection effects

Convection effects in the membrane system in relation to volume osmotic flows result from the comparison of the characteristics $J_{v1}^A = f(\Delta C_1, \Delta C_2 = \text{const.})$, $J_{v1}^B = f(\Delta C_1, \Delta C_2 = \text{const.})$ and $J_{v1}^A = f(\Delta C_1, \Delta C_2 = \text{const.})$, as well as $J_{v2}^A = f(\Delta C_2, \Delta C_1 = \text{const.})$, $J_{v2}^B = f(\Delta C_2, \Delta C_1 = \text{const.})$ and $J_{v2}^A = f(\Delta C_2, \Delta C_1 = \text{const.})$. The measure of convective effects is the coefficient denoted by γ_{vk} , defined by Eq. (5). Using Eqs. (3) and (4), Eq. (5), for the condition $\Delta P = 0$, can be written as

$$\left(\gamma_{vk}\right)_{\Delta P=0} = \frac{J_{vk}^A - J_{vk}^B}{J_{vk}} = \zeta_p^A \zeta_{vk}^A - \zeta_p^B \zeta_{vk}^B \quad (9)$$

In Figs. 4c and 4d the results of the calculations of the γ_{v1} and γ_{v2} coefficients obtained based on Eq. (9) were shown using curves 1–4. The results shown in Fig. 4c were calculated considering the characteristics shown in Figs. 3a and 3c, whereas the results shown in Fig. 4d considering the characteristics shown in Figs. 3b and 3d in Eq. (9). As shown in Fig. 4c, there is a point on each curve for which $\gamma_{v1} = 0$. For curve 1 this point occurs for $\Delta C_1 = 11.4 \text{ mol m}^{-3}$, for curve 2 – for $\Delta C_1 = 559.1 \text{ mol m}^{-3}$, for curve 3 – for $\Delta C_1 = 1,018.7 \text{ mol m}^{-3}$ and for curve 4 – for $\Delta C_1 = 1,502.4 \text{ mol m}^{-3}$. Additionally, as shown in Fig. 3d, there is a point on each curve for which $\gamma_{v2} = 0$. For curve 1 this point occurs for $\Delta C_2 = 1.15 \text{ mol m}^{-3}$, for curve 2 – for $\Delta C_2 = 51.6 \text{ mol m}^{-3}$, for curve 3 – for $\Delta C_2 = 90.1 \text{ mol m}^{-3}$ and for curve 4 – for $\Delta C_2 = 128.1 \text{ mol m}^{-3}$. It can be assumed that at this point the thickness of the boundary concentration layers reaches the critical value δ_1^{crit} or δ_2^{crit} . If $\gamma_{vk} > 0$, then the convective fluxes are directed anti-parallel to \mathbf{g} , and if $\gamma_{vk} < 0$ parallel to \mathbf{g} . This means that for $\gamma_{vk} < 0$ or $\gamma_{vk} > 0$ ($k = 1$ or 2), the CBLs complex becomes unstable which is manifested by convective fluxes.

4.5. Amplification of volume flux

The amplification properties of the membrane system in relation to volume fluxes result from the comparison of the respective characteristics $J_{v1}^A = f(\Delta C_1, \Delta C_2 = \text{const.})$, $J_{v1}^B = f(\Delta C_1, \Delta C_2 = \text{const.})$, $J_{v2}^A = f(\Delta C_2, \Delta C_1 = \text{const.})$ and $J_{v2}^B = f(\Delta C_2, \Delta C_1 = \text{const.})$ for ternary and binary solutions. The measure of these properties is the amplification coefficient (a_{vk}^r), as defined by the expression [19]:

$$a_{vk}^r = \frac{(\Delta J_{vk}^r)_{\text{ter.}}}{(\Delta J_{vk}^r)_{\text{bin.}}} \quad (10)$$

where $(\Delta J_{vk}^r)_{\text{ter.}}$, $(\Delta J_{vk}^r)_{\text{bin.}}$ – change of the volume flux in ternary and binary solutions, respectively, caused by the same change in concentration ΔC_k . The superscript $r = A, B$ denotes the configuration of the membrane system, while the subscript $k = 1, 2$ refers to the solution component.

Using Eqs. (3) and (4), Eq. (10) can be written as:

$$a_{v1}^r = \zeta_p^r \zeta_{v1}^r \left(1 + \frac{\varepsilon_2 \sigma_2 \Delta C_2}{\varepsilon_1 \sigma_1 \Delta(\Delta C_1)} \right) \quad (11)$$

$$a_{v2}^r = \zeta_p^r \zeta_{v2}^r \left(1 + \frac{\varepsilon_1 \sigma_1 \Delta C_1}{\varepsilon_2 \sigma_2 \Delta(\Delta C_2)} \right) \quad (12)$$

The characteristics $a_{v1}^A = f(\langle C_1 \rangle, \Delta C_2 = \text{const.})$ and $a_{v1}^B = f(\langle C_1 \rangle, \Delta C_2 = \text{const.})$ for $\Delta C_2 = 100 \text{ mol m}^{-3}$ (curves 1A and 1B), $\Delta C_2 = 200 \text{ mol m}^{-3}$ (curves 2A and 2B) and $\Delta C_2 = 300 \text{ mol m}^{-3}$ (curves 3A and 3B), shown in Fig. 5a, were calculated based on the dependences $J_{v1}^A = f(\Delta C_1, \Delta C_2 = \text{const.})$ and $J_{v1}^B = f(\Delta C_1, \Delta C_2 = \text{const.})$ shown in Fig. 3c. It is assumed that that is $\langle C_1 \rangle$ a half of the sum of two consecutive values of ΔC_1 , while $\langle C_2 \rangle$ is a half of the sum of two consecutive values of ΔC_2 . The curves 1, 2 and 3 for configuration A shown in Fig. 5a for configuration A have maxima for: $\langle C_1 \rangle = 531.25 \text{ mol m}^{-3}$, $a_{v1}^A = 20$ and $\langle C_1 \rangle = -312.5 \text{ mol m}^{-3}$, $a_{v1}^A = 110$ (curve 1), for $\langle C_1 \rangle = 968.75 \text{ mol m}^{-3}$, $a_{v1}^A = 24.75$ and $\langle C_1 \rangle = -187.575 \text{ mol m}^{-3}$, $a_{v1}^A = 98$ (curve 2) and for $\langle C_1 \rangle = 1,406.25 \text{ mol m}^{-3}$, $a_{v1}^A = 30.5$ and $\langle C_1 \rangle = -97.75 \text{ mol m}^{-3}$, $a_{v1}^A = 80$ (curve 3). Therefore, for ternary solutions J_{v1}^A is much larger than J_{v1}^A for binary solutions. The curves 1, 2 and 3 for configuration B shown in Fig. 10 also have minima for $\langle C_1 \rangle = -562.5 \text{ mol m}^{-3}$, $a_{v1}^B = -190$ (curve 1), for $\langle C_1 \rangle = -1,062, 5 \text{ mol m}^{-3}$, $a_{v1}^B = -150$ (curve 2) and for $\langle C_1 \rangle = -1,562.5 \text{ mol m}^{-3}$, $a_{v1}^B = -95$ (curve 3). A positive amplification factor indicates that depending on the configuration of the membrane system, the tested membrane setup has a positive or a negative feedback in the range of J_{v1}^A generation generated by ΔC_1 and controlled by ΔC_2 .

The characteristics of $a_{v2}^A = f(\langle C_2 \rangle, \Delta C_1 = \text{const.})$ and $a_{v2}^B = f(\langle C_2 \rangle, \Delta C_1 = \text{const.})$ for $\Delta C_1 = 250 \text{ mol m}^{-3}$ (curves 1A and 1B), $\Delta C_1 = 500 \text{ mol m}^{-3}$ (curves 2A and 2B) and $\Delta C_1 = 750 \text{ mol m}^{-3}$ (curves 3A and 3B), shown in Fig. 5b were calculated based on the dependences $J_{v2}^A = f(\Delta C_1, \Delta C_2 = \text{const.})$ and $J_{v2}^B = f(\Delta C_1, \Delta C_2 = \text{const.})$ presented in Fig. 3d.

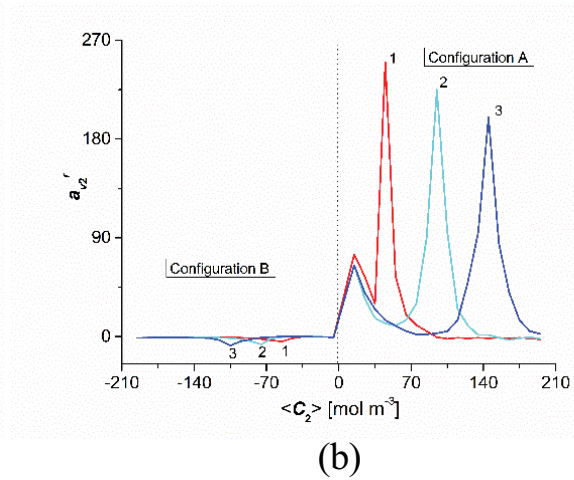
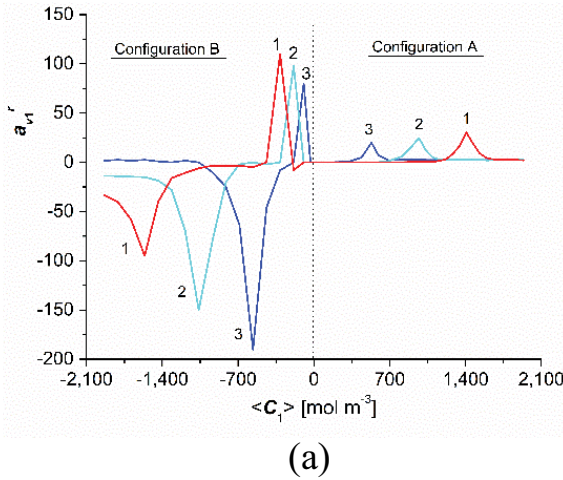


Fig. 5. Amplification of volume flux. (a) Dependences $a_{v1}^A = f(\langle C_1 \rangle)$ and $a_{v1}^B = f(\langle C_1 \rangle)$ for solutions of NH_4OH in aqueous solution H_2SO_4 and configuration A and B of the membrane system. (b) Dependence $a_{v2}^A = f(\langle C_2 \rangle)$ and $a_{v2}^B = f(\langle C_2 \rangle)$ for solutions of H_2SO_4 in aqueous solution NH_4OH and configuration A and B of the membrane system.

Curves 1, 2 and 3 for configuration A shown in Fig. 4b have maxima for $\langle C_2 \rangle = 45 \text{ mol m}^{-3}$, $a_{v2}^A = 250$ (curve 1), for $\langle C_2 \rangle = 95 \text{ mol m}^{-3}$, $a_{v2}^A = 225$ (curve 2) and for $\langle C_2 \rangle = 145 \text{ mol m}^{-3}$, $a_{v2}^A = 200$ (curve 3). Moreover, these curves have a common maximum for the maximum $\langle C_2 \rangle = 15 \text{ mol m}^{-3}$, $a_{v2}^A = 70$. Moreover, the curves 1, 2 and 3 for configuration B shown in Fig. 4b have maxima for $\langle C_2 \rangle = -55 \text{ mol m}^{-3}$, $a_{v2}^A = -4.5$ (curve 1), for $\langle C_2 \rangle = -75 \text{ mol m}^{-3}$, $a_{v2}^A = -7$ (curve 2) and for $\langle C_2 \rangle = -95 \text{ mol m}^{-3}$, $a_{v2}^A = -8$ (curve 3). A positive amplification factor indicates that depending on the configuration of the membrane system the tested membrane system has a positive or negative feedback in terms of generating the J_{v2}^B volume flux by ΔC_2 and controlled by ΔC_1 . Qualitatively similar results were obtained for ammonia solutions in an aqueous HCl solution and HCl solutions in an aqueous ammonia solution [21].

4.6. Rate of S-entropy production in concentration polarization conditions for ternary solutions

The source of entropy was calculated based on Eq. (6) for the homogeneity conditions of the solutions $(\Phi_S)_{J_{vk}}$ and based on Eq. (8) for the concentration polarization conditions, assuming the condition $\Delta P = 0$. The dependencies $(\Phi_S)_{J_{v1}} = f(\Delta C_1, \Delta C_2 = \text{const.})$ were illustrated in Fig. 6a and dependencies $(\Phi_S)_{J_{v2}} = f(\Delta C_2, \Delta C_1 = \text{const.})$ in Fig. 6b. As shown in Fig. 6A, for all values of ΔC_2 the curves 1A–4A and the curves 1B–4B are centrally symmetrical with respect to the vertical axis passing through the point $\Delta C_1 = 0$. Analogously, for all values of ΔC_1 the curves 1B–4B and the curves 1A–4A shown in Fig. 6b are centrally symmetrical with respect to the vertical axis passing through the point $\Delta C_2 = 0$.

The source of entropy for the concentration polarization conditions was calculated based on Eq. (8), assuming $\Delta P = 0$. The dependencies $(\Phi_S^A)_{J_{v1}^A} = f(\Delta C_1, \Delta C_2 = \text{const.})$ and $(\Phi_S^B)_{J_{v1}^B} = f(\Delta C_1, \Delta C_2 = \text{const.})$ were presented in

Fig. 6c and dependencies $(\Phi_S^A)_{J_{v2}^A} = f(\Delta C_2, \Delta C_1 = \text{const.})$ and $(\Phi_S^B)_{J_{v2}^B} = f(\Delta C_2, \Delta C_1 = \text{const.})$ were presented in Fig. 6d.

For all values of ΔC_2 , the curves 1A–4A and the curves 1B–4B shown in Fig. 6d are centrally asymmetric with respect to the vertical axis passing through the point $\Delta C_1 = 0$. Analogously, for all values of ΔC_1 the graphs 1B–4B and the curves 1A–4A shown in Fig. 6e are centrally asymmetric with respect to the vertical axis passing through the point $\Delta C_2 = 0$.

Using Eqs. (3) and (4), the Eqs. (6) and (8) for osmotic transport can be written as:

$$\begin{aligned} (\Phi_S^r)_{J_{vk}} &= \frac{1}{T} \left(J_{vk}^r \sum_{k=1}^2 \pi_k \right) \\ &= L_p \zeta_p^r \zeta_{vk}^r R^2 T \left(\sum_{k=1}^2 \varepsilon_k \sigma_k \Delta C_k^2 + \sum_{k=1}^2 \varepsilon_k \sigma_k \prod_{k=1}^2 \Delta C_k \right) \end{aligned} \quad (13)$$

$$\begin{aligned} (\Phi_S)_{J_{vk}} &= \frac{1}{T} \left(J_{vk} \sum_{k=1}^2 \pi_k \right) \\ &= L_p R^2 T \left(\sum_{k=1}^2 \varepsilon_k \sigma_k \Delta C_k^2 + \sum_{k=1}^2 \varepsilon_k \sigma_k \prod_{k=1}^2 \Delta C_k \right) \end{aligned} \quad (14)$$

Subtracting the sides of Eqs. (14) and (13) can be written as:

$$\begin{aligned} \Delta \Phi_{Sk}^r &= (\Phi_S)_{J_{vk}} - (\Phi_S^r)_{J_{vk}} \\ &= L_p R^2 T \left(\sum_{k=1}^2 \varepsilon_k \sigma_k \Delta C_k^2 + \sum_{k=1}^2 \varepsilon_k \sigma_k \prod_{k=1}^2 \Delta C_k \right) (1 - \zeta_p^r \zeta_{vk}^r) \end{aligned} \quad (15)$$

where: $\Delta \Phi_{Sk}^r$ is a measure of the concentration polarization effect of the entropy source.

The dependencies $\Delta \Phi_{S1}^r = f(\Delta C_1, \Delta C_2 = \text{const.})$ shown in Fig. 6e were obtained by subtracting the results of

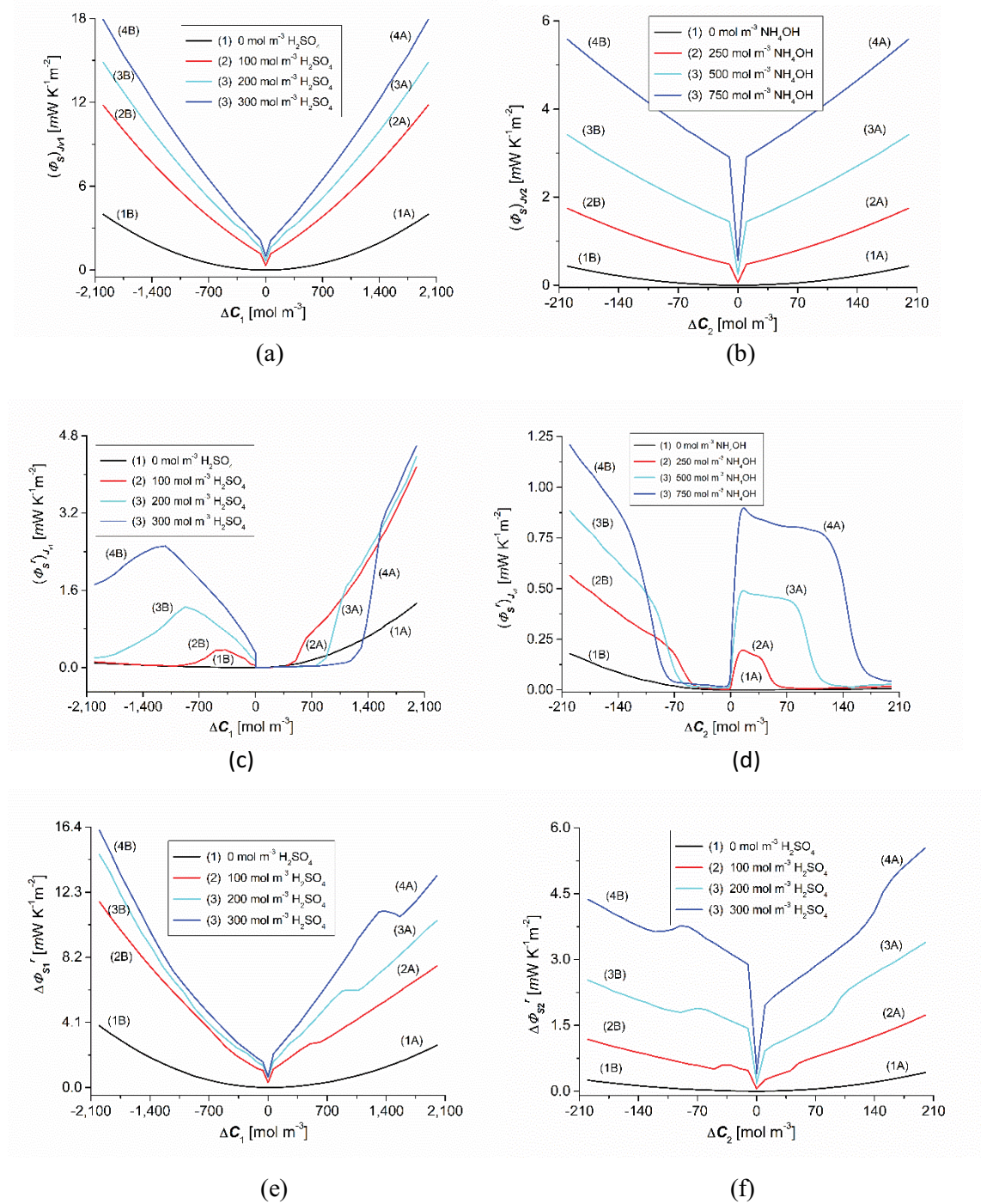


Fig. 6. S-entropy production rate under concentration polarization conditions for ternary solutions. (a) Experimental dependence $(\Phi_s)_{J_{s1}} = f(\Delta C_1, \Delta C_2 = \text{const.})$ for solutions of $\text{NH}_3 \cdot \text{H}_2\text{O}$ in aqueous solution H_2SO_4 for the conditions of homogeneity of solutions separated by the membrane. (b) Experimental dependence $(\Phi_s)_{J_{s2}} = f(\Delta C_2, \Delta C_1 = \text{const.})$ for solutions of H_2SO_4 in aqueous solution $\text{NH}_3 \cdot \text{H}_2\text{O}$ for the conditions of homogeneity of solutions separated by the membrane. (c) Experimental dependence $(\Phi_s^r)_{J_{s1}} = f(\Delta C_1, \Delta C_2 = \text{const.})$, ($r = A, B$) for solutions of $\text{NH}_3 \cdot \text{H}_2\text{O}$ in aqueous solution H_2SO_4 and configuration A and B of the membrane system in concentration polarization conditions. (d) Experimental dependence $(\Phi_s^r)_{J_{s2}} = f(\Delta C_2, \Delta C_1 = \text{const.})$ ($r = A, B$) for solutions of H_2SO_4 in aqueous solution of $\text{NH}_3 \cdot \text{H}_2\text{O}$ and configuration A and B of the membrane system in concentration polarization conditions. (e) Experimental dependence $\Delta\Phi_{s1}^r = f(\Delta C_1, \Delta C_2 = \text{const.})$ ($r = A, B$) for solutions of $\text{NH}_3 \cdot \text{H}_2\text{O}$ in aqueous solution H_2SO_4 and configuration A and B of the membrane system. (f) Experimental dependence $\Delta\Phi_{s2}^r = f(\Delta C_2, \Delta C_1 = \text{const.})$ ($r = A, B$) for solutions of H_2SO_4 in aqueous $\text{NH}_3 \cdot \text{H}_2\text{O}$ solution and configuration A and B of the membrane system.

Table 1

Coefficients ζ_{v1}^r and concentration Rayleigh numbers R_{Cl}^r for certain values of ΔC_1 and $\Delta C_2 = \text{const.}$

ΔC_1 (mol m ⁻³)	ΔC_2 (mol m ⁻³)	ζ_{v1}^A	ζ_{v1}^B	γ_{v1}	R_{Cl}^A	R_{Cl}^B
812.5	200	0.015	0.235	-0.171	1.57×10^6	148.74
875	200	0.023	0.215	-0.192	3.6×10^5	183.53
950	200	0.05	0.177	-0.127	2.48×10^4	314.73
1,000	200	0.08	0.137	-0.057	4,390.47	678.88
1,020	200	0.117	0.117	0	1,089.86	1,089.86
1,062.5	200	0.17	0.09	0.12	222.663	2,168.32
1,125	200	0.21	0.07	0.14	61.92	3,211.02
1,250	200	0.237	0.046	0.191	-14.51	-1,643.74
200	0.268	0.027	0.241	-52.56	-1.6×10^5	-3.76×10^4

$\Delta\Phi_{s1}^r = f(\Delta C_1, \Delta C_2 = \text{const.})$ shown in Fig. 6c from the corresponding results of $(\Phi_s)_{f_{v1}} = f(\Delta C_1, \Delta C_2 = \text{const.})$ presented in Fig. 6a. The dependencies $\Delta\Phi_{s2}^r = f(\Delta C_2, \Delta C_1 = \text{const.})$ shown in Fig. 6f were obtained by subtracting the results of $(\Phi_s)_{f_{v2}}^r = f(\Delta C_2, \Delta C_1 = \text{const.})$ presented in Fig. 6d from the corresponding results of $(\Phi_s)_{f_{v2}} = f(\Delta C_2, \Delta C_1 = \text{const.})$ presented in Fig. 6b. For all values of ΔC_2 , the curves 1A–4A and 1B–4B are centrally asymmetric with respect to the vertical axis passing through the point $\Delta C_1 = 0$ (Fig. 6e). Similarly, for all values of ΔC_1 , the curves 1B–4B and 1A–4A are centrally asymmetric with respect to the vertical axis passing through the point $\Delta C_2 = 0$ (Fig. 6f).

For the Nephrophan[®] membrane, $\zeta_p^r = 1$, whereas ζ_{vk}^r may depend on the following parameters: permeability coefficient of membrane (ω_k), mass density of solution (ρ) and kinematic viscosity (ν), diffusion coefficient (D_k) and concentration Rayleigh number (R_C). The coefficient ζ_{vk}^r is the quotient of J_{vk}^r/J_{vk} and can therefore be calculated from the results shown in Fig. 3a–d. The characteristic $\zeta_{v1}^r = f(\Delta C_1, \Delta C_2 = 200 \text{ mol m}^{-3})$ presented in Fig. 4a (curves 3A and 3B) was used to calculate R_{Cl}^r . As shown in Figs. 3A and 3C, $(\zeta_{v1}^A)_{\text{min.}} = 0.005$, $(\zeta_{v1}^A)_{\text{max.}} = 0.307$, $(\zeta_{v1}^B)_{\text{min.}} = 0.014$, $(\zeta_{v1}^A)_{\text{max.}} = 0.415$ and $\zeta_{v1}^A = \zeta_{v1}^B = 0.117$ ($\Delta C_1 = 1,020 \text{ mol/m}^3$) and $\gamma_{v1} = 0$.

Using the results presented in [33] for solutions containing two solutes, it is possible to write:

$$R_{Cl}^r = \alpha_l \left[\frac{\partial \rho}{\partial C_1} \beta_1 \Delta C_1 + \frac{\partial \rho}{\partial C_2} \beta_2 \Delta C_2 \right] \frac{(1 - \zeta_1^r)^4}{\zeta_1^r} \quad (16)$$

$$\text{where: } \alpha_l = \frac{g(D_1)^3}{16(RT)^3(\omega_1)^4 \rho_l \nu_l}, \beta_1 = \frac{\omega_1 \varepsilon_1}{D_1}, \beta_2 = \frac{\omega_2 \varepsilon_2}{D_2}.$$

As shown in the above equation, the sign R_{Cl}^r depends on the sign of $\partial \rho / \partial C_k$ ($k = 1$ or 2) because α_l , β_1 , β_2 and ζ_1^r are always greater than zero. If $\partial \rho / \partial C_1 < 0, \partial \rho / \partial C_2 > 0$ and $\left(\frac{\partial \rho}{\partial C_1} \beta_1 \Delta C_1 + \frac{\partial \rho}{\partial C_2} \beta_2 \Delta C_2 \right) < 0$, it $R_{Cl}^r < 0$. $R_{Cl}^r = 0$, then, if $\left(\frac{\partial \rho}{\partial C_1} \beta_1 \Delta C_1 + \frac{\partial \rho}{\partial C_2} \beta_2 \Delta C_2 \right) = 0$.

If in turn $\left(\frac{\partial \rho}{\partial C_1} \beta_1 \Delta C_1 + \frac{\partial \rho}{\partial C_2} \beta_2 \Delta C_2 \right) > 0$, then $R_{Cl}^r > 0$.

Considering the following data in Eq. (16): $g = 9.81 \text{ m s}^{-2}$, $\partial \rho / \partial C_1 = -0.013 \text{ kg mol}^{-1}$, $\partial \rho / \partial C_2 = 0.054 \text{ kg mol}^{-1}$, $\omega_1 = 2.7 \times 10^{-9} \text{ mol N}^{-1} \text{ s}^{-1}$, $\omega_2 = 3.0 \times 10^{-9} \text{ mol N}^{-1} \text{ s}^{-1}$, $D_1 = 1.54 \times 10^{-9} \text{ m}^2 \text{ s}^{-1}$, $D_2 = 1.15 \times 10^{-9} \text{ m}^2 \text{ s}^{-1}$, $\rho_l = 997 \text{ kg m}^{-3}$, $\nu_l = 1.01 \times 10^{-6} \text{ m}^2 \text{ s}^{-1}$, $R = 8.31 \text{ J mol}^{-1} \text{ K}^{-1}$, $T = 295 \text{ K}$, $\varepsilon_1 = \varepsilon_2 = 2$, the characteristics of $R_{Cl}^r = f(\Delta C_1, \Delta C_2 = 200 \text{ mol m}^{-3})$ were calculated and shown in Table 1. The critical value of the concentration Rayleigh number is $R_{Cl}^A = R_{Cl}^B = (R_{Cl})_{\text{crit.}} = 1089.86$ for $\Delta C_1 = 1,020 \text{ mol m}^{-3}$, $\Delta C_2 = 200 \text{ mol m}^{-3}$ (Table 1). The obtained value is comparable with the value presented in other studies [34,35]. Similar to previous membrane systems, the concentration Rayleigh number acts as a switch between the two states of the concentration field: convective (with a higher entropy source value) and non-convective (with a lower entropy source value). The operation of this switch indicates the regulatory role of Earth's gravity in relation to osmotic membrane transport.

5. Conclusions

- The concentration and orientation of water solutions of H_2SO_4 and/or ammonia in relation to a horizontally oriented membrane influence the value of volume fluxes (J_{vk}^r) under the conditions of Earth's gravity.
- J_{vk}^r are linear for concentration polarization conditions and aqueous solutions of H_2SO_4 or ammonia, whereas J_{vk}^r are a non-linear function of the differences in concentrations of the solutions for aqueous solutions of H_2SO_4 and ammonia.
- The values of J_{vk}^r are dependent, whereas the values of J_{vk} are independent, of the orientation of the solutions with respect to the horizontally oriented membrane. The following dependencies $J_{vk} > J_{vk}^r$ are satisfied for these fluxes.
- The concentration polarization coefficient ζ_i^r is related to the modified concentration Rayleigh number, that is, the parameter controlling the transition from the convective (diffusive) state to the convective state.
- The understanding of the properties and mechanism of membrane transport can be applied to the development and improvement of membrane technologies and techniques useful in medicine and in water and wastewater treatment processes.

Symbols

A	—	Area surface of membrane, m^2
a_k^r	—	Coefficients of amplification of the volume osmotic flux, $k = 1, 2$
C_{hk}, C_{lk}	—	Concentration of solutions ($C_{hk} > C_{lk}$, $k = 1, 2$), $mol\ m^{-3}$
\bar{C}_k	—	Average concentration in the membrane (M) or complex $l_h^r/M/l_i^r$, $mol\ m^{-3}$
dS/dt	—	Rate of changes in the entropy of the system, $J\ K^{-1}\ s^{-1}$
dS_e/dt	—	Rate of entropy exchange between the system and the environment, $J\ K^{-1}\ s^{-1}$
dS_f/dt	—	Rate of entropy formation inside the system, $J\ K^{-1}\ s^{-1}$
D_k	—	Diffusion coefficient, $m^2\ s^{-1}$
F	—	Free energy, J
g	—	Gravity acceleration, $m\ s^{-2}$
J_k	—	Solute fluxes for the conditions of homogeneity of solutions, $mol\ m^2\ s^{-1}$
J_{vk}	—	Volume fluxes for the conditions of homogeneity of solutions, $m\ s^{-1}$
J_{vk}^r	—	Volume fluxes or the conditions of concentration polarization of solutions, $m\ s^{-1}$
J_k^r	—	Solute flux for the conditions of concentration polarization of solutions, $mol\ m^{-2}\ s^{-1}$
$l_h^r/M/l_i^r$	—	Complex of concentration boundary layers (l_h^r, l_i^r) and membrane, M
L_p	—	Hydraulic permeability coefficient, $m^3\ N^{-1}\ s^{-1}$
P	—	Hydrostatic pressure, Pa
r	—	Configuration of the membrane system, $r = A, B$
R	—	Gas constant, $R = 8.31\ J\ mol^{-1}\ K^{-1}$
R_C	—	Concentration Rayleigh number
S	—	S-entropy, $J\ K^{-1}$
TS	—	Dispersed energy, J
T	—	Absolute temperature, K
U	—	Internal energy, J
V	—	Volume, m^3
X_k	—	Thermodynamic forces
δ_h^r, δ_l^r	—	Thicknesses of the concentration boundary layers, m
π_k	—	Osmotic pressures of k -th solute ($k = 1, 2$), Pa
x	—	Thickness of membrane, m
φ_s	—	Source of entropy, $W\ K^{-1}\ m^{-3}$
Φ_{Sk}	—	Source of S-entropy for the membrane, $W\ K^{-1}\ m^{-2}$
Φ_S^r	—	S-entropy source for the concentration polarization conditions, $W\ K^{-1}\ m^{-2}$
$(\Phi_{Sk}^r)_{J_{ik}}$	—	S-entropy produced by J_{vk}^r , $W\ K^{-1}\ m^{-2}$
$(\Phi_{Sk}^r)_{J_k}$	—	S-entropy produced by J_k^r , $W\ K^{-1}\ m^{-2}$
Φ_S^r	—	S-entropy source for the concentration polarization conditions, $W\ K^{-1}\ m^{-2}$
$(\Phi_S^r)_{J_{ik}^r}$	—	S-entropy produced by J_{vk}^r , $W\ K^{-1}\ m^{-2}$
$(\Phi_S^r)_{J_k^r}$	—	S-entropy produced by J_k^r , $W\ K^{-1}\ m^{-2}$
γ_k	—	Coefficient of convection effects
$\zeta_{pr}^r, \zeta_{vk}^r$	—	Hydraulic and osmotic concentration polarization coefficients
σ_k	—	Reflection coefficient

ω_k	—	Permeability coefficient, $mol\ N^{-1}\ s^{-1}$
ε_k	—	Van't Hoff coefficient
ρ	—	Mass density of solution, $kg\ m^{-3}$
ν	—	Kinematic viscosity, $m^2\ s^{-1}$

Acknowledgements

The scientific research was funded both by the statute subvention of Czestochowa University of Technology, Jan Dlugosz University in Czestochowa, University of Economics in Katowice and Silesian University of Technology.

References

- [1] E. Boeker, R. van Grondelle, Environmental Physics, John Wiley & Sons, Chichester, 1999.
- [2] B. Lipton, The Biology of Belief: Unleashing the Power of Consciousness, Hay House, Carsband, 2018.
- [3] K.M. Batko, A. Slezak, W.M. Bajdur, The role of gravity in the evolution of the concentration field in the electrochemical membrane cell, Entropy, 22 (2020) 680, doi: 10.3390/e22060680.
- [4] R. Baker, Membrane Technology and Application, John Wiley & Sons, New York, 2012.
- [5] S.P. Nunes, P.Z. Culfaz-Emecen, G.Z. Ramon, T. Visser, G.H. Koops, W. Jin, M. Ulbricht, Thinking the future of membranes: perspectives for advanced and new membrane materials and manufacturing processes, J. Membr. Sci., 598 (2020) 117761, doi: 10.1016/j.memsci.2019.117761.
- [6] D. Lasrado, S. Ahankari, K. Kar, Nanocellulose-based polymer composites for energy applications—a review, J. Appl. Polym. Sci., 137 (2020) 48959, doi: 10.1002/app.48959.
- [7] T.P.N. Nguyen, B.-M. Jun, J. Hwa Lee, Y.-N. Kwon, Comparison of integrally asymmetric and thin film composite structures for a desirable fashion of forward osmosis membranes, J. Membr. Sci., 495 (2015) 457–470.
- [8] T.P.N. Nguyen, B.-M. Jun, Y.-N. Kwon, The chlorination mechanism of integrally asymmetric cellulose triacetate (CTA)-based and thin film composite polyamide-based forward osmosis membrane, J. Membr. Sci., 523 (2017) 111–121.
- [9] Y. Seo, Y.-C. Jung, M.-S. Park, D.-W. Kim, Solid polymer electrolyte supported by porous polymer membrane for all-solid-state lithium batteries, J. Membr. Sci., 603 (2020) 117995, doi: 10.1016/j.memsci.2020.117995.
- [10] Y. Demirel, Non-equilibrium Thermodynamics: Transport and Rate Processes in Physical and Biological System, Amsterdam, Elsevier, 2002.
- [11] D. Kondepudi, Introduction to Modern Thermodynamics, John Wiley & Sons, Chichester, 2008.
- [12] A. Katchalsky, P.F. Curran, Non-equilibrium Thermodynamics in Biophysics, Harvard, Cambridge, 1965.
- [13] Y. Demirel, S.I. Sandler, Thermodynamics and bioenergetics, Biophys. Chem., 97 (2002) 87–111.
- [14] M. Delmotte, J. Chanu, Non-Equilibrium Thermodynamics and Membrane Potential Measurement in Biology, G. Millazzo, Ed., Topics Bioelectrochemistry and Bioenergetics, John Wiley & Sons, Chichester, 1979, pp. 307–359.
- [15] A. Slezak, I. Slezak-Prochazka, S. Grzegorzczyn, J. Jasik-Slezak, Evaluation of S-entropy production in a single-membrane system in concentration polarization conditions, Transp. Porous Media, 116 (2017) 941–957.
- [16] A. Slezak, S. Grzegorzczyn, K.M. Batko, W. Pilis, R. Biczak, Membrane transport in concentration polarization conditions: evaluation of S-entropy production for ternary non-electrolyte solutions, J. Non-Equilib. Thermodyn., 45 (2020) 385–399.
- [17] A. Slezak, Irreversible thermodynamic model equations of the transport across a horizontally mounted membrane, Biophys. Chem., 34 (1989) 91–102.
- [18] A. Slezak, J. Jasik-Slezak, S. Grzegorzczyn, I. Slezak-Prochazka, Nonlinear effects in osmotic volume flows of electrolyte solutions through double-membrane system, Transp. Porous Media, 92 (2012) 337–356.

- [19] A. Ślęzak, J. Jasik-Ślęzak, J. Wąsik, A. Sieroń, W. Pilis, Volume osmotic flows of non-homogeneous electrolyte solutions through horizontally mounted membrane, *Gen. Physiol. Biophys.*, 21 (2002) 115–146.
- [20] A. Ślęzak, S. Grzegorzyn, K.M. Batko, W.M. Bajdur, M. Włodarczyk-Makula, Applicability of the L' form of the Kedem–Katchalsky–Peusner equations for membrane transport in water purification technology, *Desal. Water Treat.*, 202 (2020) 48–60.
- [21] K.M. Batko, A. Ślęzak, Evaluation of the global S-entropy production in membrane transport of aqueous solutions of hydrochloric acid and ammonia, *Entropy*, 22 (2020) 1021, doi: 10.3390/e22091021.
- [22] A. Ślęzak, S. Grzegorzyn, J. Jasik-Ślęzak, K. Michalska-Małecka, Natural convection as an asymmetrical factor of the transport through porous membrane, *Transp. Porous Media*, 84 (2010) 685–698.
- [23] K. Dworecki, Interferometric investigation of near-membrane diffusion layers, *J. Biol. Phys.*, 21 (1995) 37–49.
- [24] K. Dworecki, S. Wąsik, A. Ślęzak, Temporal and spatial structure of the concentration boundary layers in a membrane system, *Physica A*, 326 (2003) 360–369.
- [25] K. Dworecki, T. Kosztołowicz, St. Mrówczyński, S. Wąsik, Time evolution of near membrane layers, *Eur. J. Phys. E*, 3 (2000) 389–394.
- [26] K. Dworecki, A. Ślęzak, B. Ornal-Wąsik, S. Wąsik, Effect of hydrodynamic instabilities on solute transport in a membrane system, *J. Membr. Sci.*, 265 (2005) 94–100.
- [27] S. Grzegorzyn, A. Ślęzak, K. Michalska-Małecka, I. Ślęzak-Prochazka, Conditions of hydrodynamic instability appearance in fluid thin layers with changes in time thickness and density gradient, *J. Non-Equilib. Thermodyn.*, 37 (2012) 77–99.
- [28] B.A. Puthenveetil, J.H. Arakeri, Plume structure in high-Rayleigh-number convection, *J. Fluid Mech.*, 542 (2005) 217–249.
- [29] B.A. Puthenveetil, G.S. Gunasegarane, Y.K. Agrawal, D. Schmeling, J. Bosbach, J.H. Arakeri, Length of near-wall plumes in turbulent convection, *J. Fluid Mech.*, 685 (2011) 335–364.
- [30] K. Batko, I. Ślęzak-Prochazka, S. Grzegorzyn, A. Ślęzak, Membrane transport in concentration polarization conditions: network thermodynamics model equations, *J. Porous Media*, 17 (2014) 573–586.
- [31] H. Klinkman, M. Holtz, W. Willgerodt, G. Wilke, D. Schoenfelder, Nephrophan® – Eine Neue Dialysemembran, *Z. Urol. Nephrol.*, 62 (1969) 285–292.
- [32] P.J. Durrant, B. Durrant, *Introduction to Advanced Inorganic Chemistry*, John Wiley and Sons, New York, 1962.
- [33] A. Ślęzak, K. Dworecki, J. Jasik-Ślęzak, J. Wąsik, Method to determine the critical concentration Rayleigh number in isothermal passive membrane transport processes, *Desalination*, 168 (2004) 397–412.
- [34] G. Lebon, D. Jou, J. Casas-Vasquez, *Understanding Non-equilibrium Thermodynamics. Foundations, Applications, Frontiers*, Springer-Verlag, Berlin-Heidelberg, 2008.
- [35] T. Lohaus, N. Herkenhoff, R. Shankar, M. Wessling, Feed flow patterns of combined Rayleigh-Bénard convection and membrane permeation, *J. Membr. Sci.*, 549 (2018) 60–66.